ACS Photonics

pubs.acs.org/journal/apchd5

Letter

Room-Temperature Lasing in a Low-Loss Tamm Plasmon Cavity

Vincent Toanen, Clémentine Symonds,* Jean-Michel Benoit, Alban Gassenq, Aristide Lemaître, and Joel Bellessa

Cite This: *ACS Photonics* 2020, 7, 2952−2957

Read Online

ACCESS | Metrics & More | Article Recommendations | Supporting Information

ABSTRACT: Optical Tamm structures offer great possibilities for the development of new optoelectronic devices ranging from polarized laser sources to plasmon generators. Indeed, thanks to the patterning of a thin metallic film alone, microscale confinement of light is achieved, which constitutes a very easy and flexible way to make confined lasers. Here, we report on room-temperature lasing of a Tamm structure, based on an original geometry with enhanced quality factor. In this so-called Super Tamm structure, a low-index dielectric layer is inserted between a silver film and an AlGaAs/AlAs distributed Bragg reflector while keeping the mode confinement at the metallic/dielectric interface. Numerical simulations of this structure show *Q*-factors up to 6500. Room-temperature lasing is achieved with this new architecture, as demonstrated by the nonlinear emission intensity increase and the spectral and emission-diagram narrowing. This result is a determinant step toward the realization of useful Tamm laser devices.

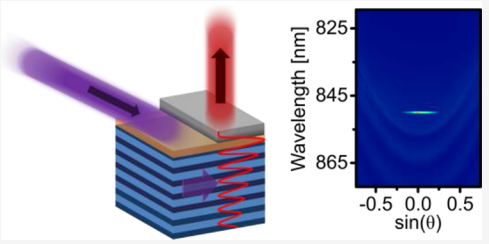

KEYWORDS: *Tamm plasmon, semiconductor laser, surface mode, hybrid metallic/semiconducting structure, microcavity, GaAs, quantum well*

The exploitation of metal in semiconductor lasers has proven to be a very efficient way to improve the device efficiency by confining light at the microscale or nanoscale level.[1−6] Metal allows to reduce the mode volume, leading to enhancement of the spontaneous emission rate and even to "threshold-less lasers".[7−9] Two different strategies can be distinguished. One approach consists in the use of plasmonic modes, which are characterized by strong nanoscale confinement of light, but at the expense of modest *Q*-factors.[3−6,10,11] Metal-coated semiconductor cavities are another strategy to make efficient and compact laser sources. In this case, metal prevents the optical mode from leaking outside of the cavity when reducing its size down to the wavelength scale or less, thus, allowing denser integration.[1,2,7,12−14] Furthermore, metallic loss can be maintained quite low, thanks to a rather small overlap between the optical mode and the metal.

Tamm plasmons, which are optical modes occurring at the interface between a distributed Bragg reflector (DBR) and a metallic layer,[15,16] are an interesting alternative, as they lie between metal−semiconductor cavities and spasers. Indeed, a Tamm mode can be seen like a cavity mode, but in a zero-thickness cavity,[15] or like a surface mode, since its field intensity decreases when moving away from the metal/semiconductor interface. Due to its surface sensitivity, the microscale confinement of light in Tamm plasmon structures is achieved thanks to easy patterning of the thin metallic layer that shapes the mode,[17−20] without resorting to any complex etching step.[21,22] This allows to design complex confinement geometries, which realization would be very challenging by etching semiconducting medium over hundreds of nanometers in a vertical cavity structure. Tamm plasmon structures have thus been proposed for various applications, such as phase-locked lasing of coherent modes,[23] electro-optical tuning of polaritons,[24] surface plasmon coupling,[25−29] guided modes propagation,[30] photonic bandgap engineering,[31] second- or third-harmonic generation enhancement,[32,33] or all-optical switching.[34,35] They are also promising for solar cells,[36] light-emitting devices,[37] and spectrally selective thermal emission.[38,39] Another key advantage of Tamm modes is that the top metallic part can also be used for electrical injection, which is promising for designing very simple Tamm-based LEDs or laser diodes. Confined optically pumped Tamm plasmon lasers have already been demonstrated with quantum wells (QW) as an active medium,[40,41] but only at cryogenic temperature, which is detrimental for applications. More recently, a modified Tamm structure has been proposed,[42] where the addition of a low-index dielectric layer between the DBR and the metallic film enables a reduction of the ohmic loss in the metal. *Q*-Factors up to 5000 were obtained in this so-called Super-Tamm structure, but at the detriment of the mode volume and its confinement at the metal/dielectric interface.

Received: May 12, 2020
Published: October 29, 2020

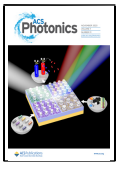

In this paper, a new Super-Tamm (ST) structure with low losses and good electric field confinement at the metal/dielectric interface is exploited to achieve room-temperature lasing. Reaching lasing operation at room temperature requires to overcome the broadening and decrease of the semiconductor gain.[43] For this purpose, a mode presenting at the same time reduced losses and a strong confinement of the field in the gain region, namely, close to the interface, is proposed. We first describe with transfer-matrix calculations the properties of this new structure. We then perform reflectivity measurements on a ST sample to check the properties of its optical modes. Finally, we investigate the luminescence of the sample under pulsed optical pumping and demonstrate lasing operation at room temperature, which is a key point for the realization of practical Tamm laser devices.

We first compute the properties of a ST structure and compare it to a conventional Tamm plasmon structure. The structure consists of a 50 pairs $Al_{0.2}Ga_{0.8}As/AlAs$ DBR, which the photonic stopband is centered on $\lambda_B = 800$ nm, covered by a low-index SiO_2 layer and a silver layer, with thicknesses d_{SiO_2} and d_{Ag}. The addition of this low-index layer aims at reducing the intensity of the electric field in the metallic film and, thus, the losses. If the low-index layer is added without any change in the DBR structure, this reduction is made at the expense of a shift of the electric field maximum within the DBR[42] (see Supporting Information). Here, to have at the same time low losses and a mode well confined at the interface, we also modified the semiconductor part of the sample by thinning the top AlGaAs DBR layer (with thickness d_1' and optical index n_1) in order to preserve the round-trip phase condition of the Tamm mode. As a result, the effective thickness of the two last layers under silver has to be $n_1 d_1' + n_{SiO_2} d_{SiO_2} = \lambda_B/4$ and is equivalent to a conventional DBR layer for the phase evolution of a traveling wave. An equal repartition between AlGaAs and SiO_2 maximizes the Q-factor of the ST mode (see Supporting Information). So we chose $d_1' = d_1/2 = \lambda_B/8n_1$, where d_1 is the thickness of a full AlGaAs layer and $d_{SiO_2} = \lambda_B/8n_{SiO_2}$.

Values of optical indexes are taken from Johnson and Christy's data for silver[44] and from the work of Gehrsitz et al. for $Al_xGa_{1-x}As$.[45] Losses of nonmetallic materials are neglected. Figure 1a,c shows the reflectivity spectra of both conventional and ST structures for $d_{Ag} = 50$ nm. One can see on the simulated reflectivity spectra that the Tamm mode wavelength λ_T only differs by 0.5 nm between both structures. Furthermore, the electric field distribution is very similar in both structures, with the field well confined around the metal/dielectric interface (Figure 1e,f), unlike the ST modes presented in a previous work.[42] Defining the field intensity extension of the mode as $L_{mode} = \int_0^\infty |E_{mode}(z)|^2 dz/|E_{mode,max}|^2$, we find very similar extensions in both structures, with $L_{ST}/L_{Tamm} \simeq 1.1$. Here, z is the direction perpendicular to the layers and $z = 0$ corresponds to the air/metal interface. But the presence of the low index SiO_2 layer between the DBR and the silver layer modifies the electric field distribution close to the DBR−silver interface. To quantify this effect, we define the ratio of the ST field intensity extension in silver over the same extension for the conventional Tamm mode as

$$r_{ST/Tamm} = \frac{\int_0^{d_{Ag}} |E_{ST}(z)|^2 dz/|E_{ST,max}|^2}{\int_0^{d_{Ag}} |E_{Tamm}(z)|^2 dz/|E_{Tamm,max}|^2}$$

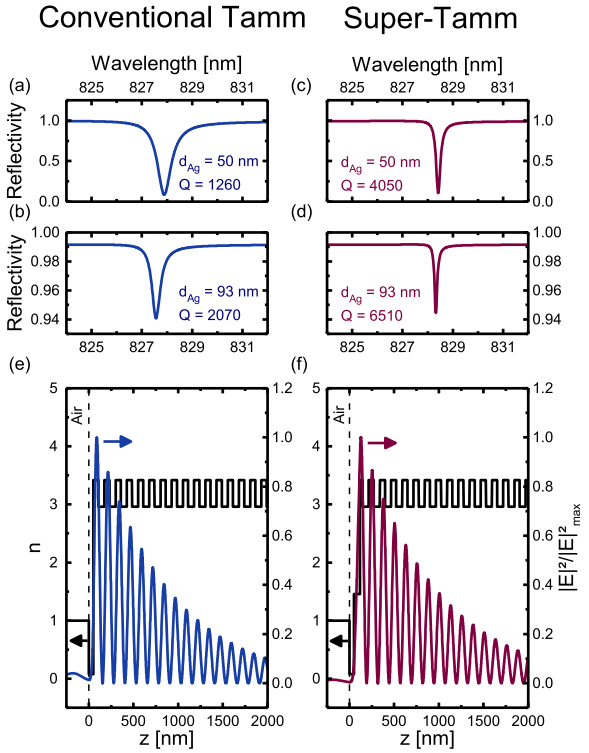

Figure 1. Transfer-matrix simulations at normal incidence. (a, b) Reflectivity spectra of a conventional Tamm structure (without SiO_2) with a 50 (a) and 93 nm (b) silver thickness. (c, d) Reflectivity spectra of a Super-Tamm (ST) structure (with SiO_2 and a reduced last DBR layer) with a 50 (c) and 93 nm (d) silver thickness. (e, f) Index profile and longitudinal distribution of the electric field intensity at normal incidence in a conventional (e) and ST (f) structure, with $d_{Ag} = 50$ nm.

We find that $r_{ST/Tamm} \simeq 0.3$, proving that the ST architecture helps reduce the fraction of the electric field lying in the metal. This results in a significant decrease in the nonradiative metal loss for the ST mode and, consequently, an increase in the quality factor, which is deduced from the reflectivity peak width. For $d_{Ag} = 50$ nm, we found that the Q-factor of the conventional mode is 1260, compared to 4050 for the ST structure. In addition, further enhancement of the Q-factor can be obtained by increasing the silver layer thickness, the latter determining the amount of radiative loss. When choosing the silver thickness to 93 nm, we computed a theoretical Q-factor of 2070 for the conventional structure and 6510 for the ST structure (Figure 1b,d). It is noteworthy that the Tamm resonance wavelength is almost exactly the same for both silver thicknesses. However, the Q-factor enhancement is made at the expense of the coupling between the mode and the propagating waves. It can be seen as a drastic reduction of the reflectivity peak depth, which is now about 5%, compared to more than 85% with 50 nm of silver. These small values will make the Tamm resonance with a thick silver film very difficult to measure in reflectometry.

To experimentally investigate the properties of this Super-Tamm mode, a 50 pairs $Al_{0.2}Ga_{0.8}As/AlAs$ DBR was grown by molecular beam epitaxy (MBE) on a GaAs substrate. A sketch of the sample is shown in Figure 2a. The 45 bottom pairs are regular pairs of quarter wavelength layers, with $d_{AlGaAs} = 57.7$ nm and $d_{AlAs} = 66.8$ nm, which corresponds to $\lambda_B = 800$ nm. Two 10 nm GaAs quantum wells are inserted in each AlGaAs

https://dx.doi.org/10.1021/acsphotonics.0c00781
ACS Photonics 2020, 7, 2952−2957

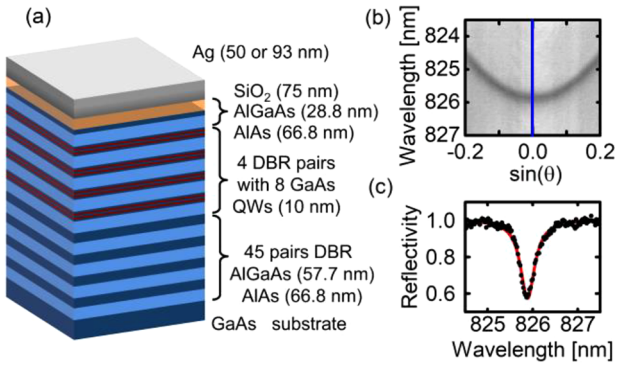

Figure 2. (a) Sketch of the ST sample. (b) Angle-resolved reflectivity measurement of a ST mode at T = 77 K, with a wavelength largely detuned from the QW absorption. Silver thickness is 50 nm. (c) Reflectivity profile along the blue line in (b). Red line is a Lorentzian fit of the experimental data.

layer of the four upper pairs, close to the maxima of the electric field. A detailed description of the QW structure is given in Supporting Information. Finally, the last top pair is composed of a regular AlAs layer and half of a regular AlGaAs layer. A 75 nm thick SiO_2 layer was deposited on the top of the DBR by plasma-enhanced chemical vapor deposition (PECVD), to complete the last layer of the DBR. Silver was then evaporated, with two different thicknesses on two adjacent areas of the same sample (d_{Ag} = 50 or 93 nm). Note that a thickness gradient along the sample was induced during MBE growth, which allows to choose the center of the photonic stopband λ_B and, consequently, tune the Tamm mode wavelength λ_T, with no significant impact on the QW excitons wavelength λ_X.

Before looking at the emission properties of this ST sample, optical reflectivity measurements have been carried out to investigate the properties of its optical modes. A broad-spectrum white source is focused on the sample, which is placed in a cryostat, with a ×50 microscope objective of numerical aperture NA = 0.75. Reflected light is then collected by the same objective and focused either on a CCD camera for direct visualization or on the entrance slit of a spectrometer. An intermediate lens, which front focal plane coincides with the Fourier plane of the objective, allows to record angle-resolved measurements, thus, giving access to the dispersion relation of the optical modes when used with the spectrometer. Figure 2b and c, respectively, shows the angle-resolved and normal incidence reflectivity spectrum of a ST mode, obtained from a 50 nm silver deposit zone. To avoid spectral broadening of the mode due to QW absorption, we cooled down the sample to 77 K to move away the excitonic transition at λ_X far from the Tamm resonance at λ_T. Measuring the width of the reflectivity dip at normal incidence, we deduced an experimental quality factor $Q \simeq 2100$.

The sample emission properties at room temperature are now investigated through photoluminescence experiments. To reach laser effect, optical gain is needed, which requires an efficient absorption of the incident light in the QWs. In a standard pumping scheme, where an excitation laser beam is directly focused on silver, absorption is very inefficient, because the silver layer reflects most of the incident light, resulting in an effective absorption rate in the QWs of ∼0.05% (estimated with transfer matrix simulations).[40] Note that this is not a fundamental limit for Tamm applications, since Tamm devices are particularly well-suited for electrical injection, which should be considerably more efficient.

In our case, to avoid the issue of inefficient optical pumping through silver, a remote excitation method, sketched in Figure 3a, was used. A mode-locked Ti:sapphire laser beam is focused

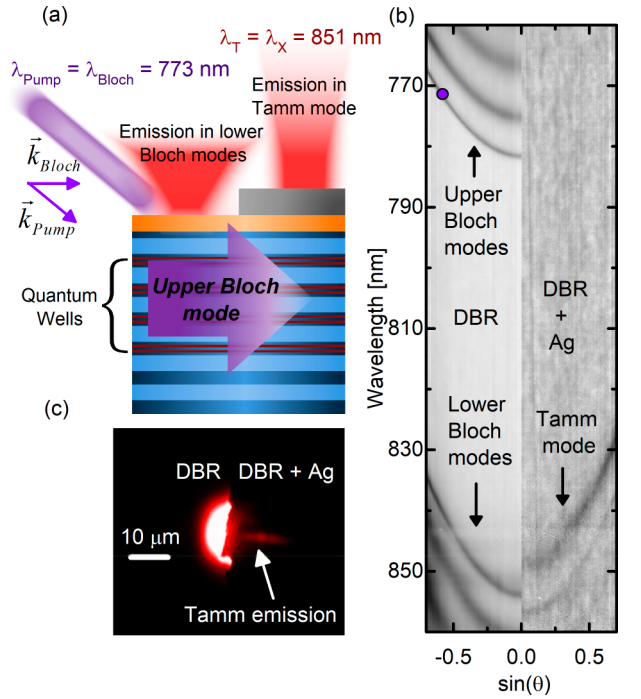

Figure 3. (a) Sketch of the excitation process. Pump laser is focused on the silver-free side, with a high incident angle ≃45° so that it matches the wave-vector of an upper Bloch mode in the DBR. This Bloch mode, marked with a purple dot in (b), propagates toward the silver-coated area and creates excitons in the QWs. Exciton emission is partly released in the tuned ST mode, and collected through the silver film. (b) Reflectivity images of the uncovered DBR region (left) and Ag-covered ST region (right). This measurement was made very close to the point where luminescence experiments were carried out, to have a small variation in the DBR thicknesses and, thus, similar modes wavelengths. (c) Direct image of luminescence from the stripe edge. Emission from the ST mode is seen from the right silver-coated side. Incident laser reflection is cut with a 800 nm long-pass filter and a polarizer.

with the microscope objective on the edge of a microstripe etched in the silver layer. The spot diameter is ≃17 μm. Laser excitation is tuned at λ_{pump} = 773 nm, the repetition rate is 80 MHz and the pulse duration is ≃0.6 ps. A high incident angle (≃45°) is set to couple with the resonant upper Bloch mode of the DBR efficiently so that coupled light propagates under the silver layer and is absorbed in the QWs. When recombining, electron−hole pairs emit light in the Tamm mode, which is tuned at the exciton emission wavelength λ_X. Emission transmitted through silver is then collected by the same objective and is sent to the same detection line as previously described. Luminescence was collected from a thick d_{Ag} = 93 nm deposit zone to benefit from the high Q-factor of the corresponding ST mode (see Figure 1) associated with a lower lasing threshold. To identify the different optical modes in this area, we acquired reflectivity spectra (Figure 3b) from both sides of the stripe edge, but in an equivalent 50 nm thick silver deposit zone (close to the excitation point), since the Tamm mode cannot be observed by reflectivity through 93 nm of

https://dx.doi.org/10.1021/acsphotonics.0c00781
ACS Photonics 2020, 7, 2952−2957

silver. From the left side of the stripe (without silver), we observe the lower and upper Bloch modes of the DBR. From the right side, with silver, we observe a Tamm mode, 5 nm far from the first lower Bloch mode wavelength. Another dip at longer wavelength corresponds to the second order Tamm mode. Figure 3c shows a direct image of the luminescence coming from the stripe edge. It appears that luminescence coming from both the uncovered DBR (on the left of the stripe edge) and the Tamm structure (on the right) is collected.

We recorded luminescence spectra for various pump powers. Emission intensity, divided by the incident pump power, is plotted in Figure 4a. As the absorption rate is difficult to

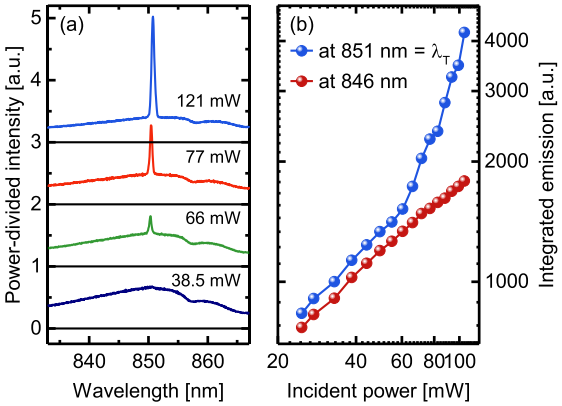

Figure 4. (a) Luminescence spectra for various pump powers. Intensity is divided by the incident pump power and arbitrarily shifted for clarity. (b) Luminescence intensity integrated around the ST wavelength at λ_T = 851 nm (blue dots) and 5 nm below (red dots), as a function of the incident pump power (log−log scale).

quantitatively evaluate with this indirect pumping scheme, spectra are associated with the incident pump power, rather than the power absorbed by the QWs. For P_{inc} = 38.5 mW, we record a broad emission of the QWs, and emission through the Tamm mode is not perceptible. Above P_{inc} = 66 mW, an emission peak appears, centered on the Tamm mode wavelength at λ_T = 851 nm. Figure 4b shows the peak intensity, integrated over a 2 nm window and plotted against the incident pump power. It is worth reminding that this integrated intensity has two contributions: emission in the Tamm mode and in the Bloch modes of same wavelength, as we collect luminescence from both sides of the stripe edge. The emission intensity evolution, at the Tamm wavelength, changes from sublinear to superlinear at $P_{threshold} \simeq 65$ mW, which suggests lasing operation. For comparison, emission intensity integrated over a shifted equivalent window, 5 nm below the peak, is shown on the same plot. One can see that there is no such a similar change in the excitation-power dependence of the emission intensity.

To confirm that this emission peak actually comes from the Tamm mode, we acquired angle-resolved luminescence spectra for several pump powers, which are shown in Figure 5. Below the threshold, at P_{inc} = 55 mW (Figure 5a), the collected luminescence is mostly emitted through the Bloch modes from the DBR side of the edge. Emission into the Tamm mode is weak below threshold since light transmission through the 93 nm thick silver film is very poor. Above threshold, for P_{inc} = 110 mW (Figure 5b), the Tamm mode spectral intensity is dominant over these of the Bloch modes. Emission in the Tamm mode is now monochromatic, with a line width $\Delta\lambda$ =

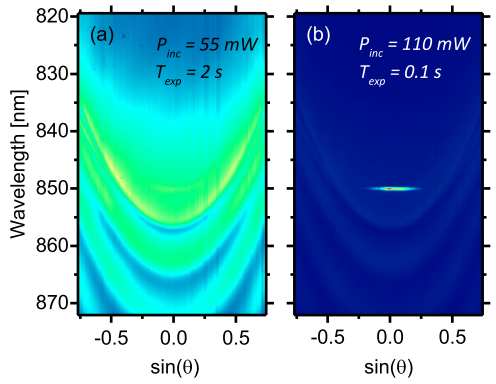

Figure 5. Angle-resolved luminescence images for two incident pump powers, below and above the lasing threshold: P_{inc} = 55 (a) and 110 mW (b).

0.37 nm, and concentrated around sin θ = 0, with a full width half-maximum angle of 10°. The spectral narrowing, the superlinear intensity increase and the narrow emission diagram around θ = 0 are clear evidence of lasing operation.

In conclusion, we demonstrated that by inserting a low-index dielectric material between the metallic film and the DBR and adjusting the thickness of the last DBR layers to conserve the round-trip phase condition, it is possible to reduce the Tamm plasmon cavity losses without losing on the mode confinement. The loss reduction gives rise to room-temperature lasing operation under pulsed optical excitation. This result confirms the great potential of Tamm plasmons for the development of new light-emitting devices. Indeed, concurrently with easy patterning of the metallic film and future electrical pumping, room-temperature operation of a Tamm structure could lead to the fabrication of many new integrated devices, such as electrically injected surface plasmon sources or complex polarization state sources.

■ ASSOCIATED CONTENT

Supporting Information

The Supporting Information is available free of charge at https://pubs.acs.org/doi/10.1021/acsphotonics.0c00781.

S1: Additional information on the Super-Tamm mode design. S2: Optimization of the relative thicknesses of the top high-index DBR layer and the low-index SiO_2 film. S3: Detailed description of the active DBR, including QWs design parameters, and electric field profile in the active layers (PDF)

■ AUTHOR INFORMATION

Corresponding Author

Clémentine Symonds − *Université de Lyon, Université Claude Bernard Lyon 1, CNRS, Institut Lumière Matière, F-69622 Lyon, France;* orcid.org/0000-0003-0925-3816; Email: clementine.symonds@univ-lyon1.fr

Authors

Vincent Toanen − *Université de Lyon, Université Claude Bernard Lyon 1, CNRS, Institut Lumière Matière, F-69622 Lyon, France*

Jean-Michel Benoit − *Université de Lyon, Université Claude Bernard Lyon 1, CNRS, Institut Lumière Matière, F-69622 Lyon, France*

https://dx.doi.org/10.1021/acsphotonics.0c00781
ACS Photonics 2020, 7, 2952−2957

Alban Gassenq − *Université de Lyon, Université Claude Bernard Lyon 1, CNRS, Institut Lumière Matière, F-69622 Lyon, France*
Aristide Lemaître − *Centre de Nanosciences et Nanotechnologies, CNRS - Université Paris-Saclay, Palaiseau, France*
Joel Bellessa − *Université de Lyon, Université Claude Bernard Lyon 1, CNRS, Institut Lumière Matière, F-69622 Lyon, France;* orcid.org/0000-0002-9525-6898

Complete contact information is available at: https://pubs.acs.org/10.1021/acsphotonics.0c00781

Notes

The authors declare no competing financial interest.

REFERENCES

(1) Hill, M. T.; Oei, Y.-S.; Smalbrugge, B.; Zhu, Y.; de Vries, T.; van Veldhoven, P. J.; van Otten, F. W. M.; Eijkemans, T. J.; Turkiewicz, J. P.; de Waardt, H.; Geluk, E. J.; Kwon, S.-H.; Lee, Y.-H.; Nötzel, R.; Smit, M. K. Lasing in metallic-coated nanocavities. *Nat. Photonics* **2007**, *1*, 589−594.
(2) Lee, J. H.; Khajavikhan, M.; Simic, A.; Gu, Q.; Bondarenko, O.; Slutsky, B.; Nezhad, M. P.; Fainman, Y. Electrically pumped sub-wavelength metallo-dielectric pedestal pillar lasers. *Opt. Express* **2011**, *19*, 21524−21531.
(3) Lu, Y.-J.; Kim, J.; Chen, H.-Y.; Wu, C.; Dabidian, N.; Sanders, C. E.; Wang, C.-Y.; Lu, M.-Y.; Li, B.-H.; Qiu, X.; Chang, W.-H.; Chen, L.-J.; Shvets, G.; Shih, C.-K.; Gwo, S. Plasmonic nanolaser using epitaxially grown silver film. *Science* **2012**, *337*, 450−453.
(4) Zhang, Q.; Li, G.; Liu, X.; Qian, F.; Li, Y.; Sum, T. C.; Lieber, C. M.; Xiong, Q. A room temperature low-threshold ultraviolet plasmonic nanolaser. *Nat. Commun.* **2014**, *5*, 1−9.
(5) Ho, J.; Tatebayashi, J.; Sergent, S.; Fong, C. F.; Iwamoto, S.; Arakawa, Y. Low-threshold near-infrared GaAs−AlGaAs core−shell nanowire plasmon laser. *ACS Photonics* **2015**, *2*, 165−171.
(6) Wei, W.; Yan, X.; Zhang, X. Ultrahigh purcell factor in low-threshold nanolaser based on asymmetric hybrid plasmonic cavity. *Sci. Rep.* **2016**, *6*, 1−7.
(7) Khajavikhan, M.; Simic, A.; Katz, M.; Lee, J. H.; Slutsky, B.; Mizrahi, A.; Lomakin, V.; Fainman, Y. Thresholdless nanoscale coaxial lasers. *Nature* **2012**, *482*, 204−207.
(8) Oulton, R. F.; Sorger, V. J.; Zentgraf, T.; Ma, R.-M.; Gladden, C.; Dai, L.; Bartal, G.; Zhang, X. Plasmon lasers at deep subwavelength scale. *Nature* **2009**, *461*, 629−632.
(9) Vyshnevyy, A. A.; Fedyanin, D. Y. Lasing threshold of thresholdless and non-thresholdless metal-semiconductor nanolasers. *Opt. Express* **2018**, *26*, 33473−33483.
(10) Liu, N.; Gocalinska, A.; Justice, J.; Gity, F.; Povey, I.; McCarthy, B.; Pemble, M.; Pelucchi, E.; Wei, H.; Silien, C.; Xu, H.; Corbett, B. lithographically defined, room temperature low threshold subwavelength red-emitting hybrid plasmonic lasers. *Nano Lett.* **2016**, *16*, 7822−7828.
(11) Ho, Y.-L.; Clark, J. K.; Kamal, A. S. A.; Delaunay, J.-J. On-chip monolithically fabricated plasmonic-waveguide Nanolaser. *Nano Lett.* **2018**, *18* (12), 7769−7776.
(12) Nezhad, M. P.; Simic, A.; Bondarenko, O.; Slutsky, B.; Mizrahi, A.; Feng, L.; Lomakin, V.; Fainman, Y. Room-temperature subwavelength metallo-dielectric lasers. *Nat. Photonics* **2010**, *4*, 395−399.
(13) Ding, K.; Liu, Z.; Yin, L.; Hill, M.; Marell, M.; van Veldhoven, P. J.; Nöetzel, R.; Ning, C.-Z. Room-temperature continuous wave lasing in deep-subwavelength metallic cavities under electrical injection. *Phys. Rev. B: Condens. Matter Mater. Phys.* **2012**, *85*, na.
(14) Ding, K.; Hill, M. T.; Liu, Z.; Yin, L.; Sahin, D.; van Veldhoven, P. J.; Geluk, E.; de Vries, T.; Ning, C.-Z. Room temperature lasing in subwavelength cylindrical metallic cavity under pulse electric injection. *Conference on Lasers and Electro-Optics (CLEO)* **2012**, *2012*, 1−2.
(15) Kaliteevski, M.; Iorsh, I.; Brand, S.; Abram, R.; Chamberlain, J.; Kavokin, A.; Shelykh, I. Tamm plasmon-polaritons: possible electromagnetic states at the interface of a metal and a dielectric bragg mirror. *Phys. Rev. B: Condens. Matter Mater. Phys.* **2007**, *76*, na.
(16) Sasin, M. E.; Seisyan, R. P.; Kaliteevski, M. A.; Brand, S.; Abram, R. A.; Chamberlain, J. M.; Egorov, A. Yu.; Vasil'ev, A. P.; Mikhrin, V. S.; Kavokin, A. V. Tamm plasmon polaritons: slow and spatially compact light. *Appl. Phys. Lett.* **2008**, *92*, 251112.
(17) Gazzano, O.; de Vasconcellos, S. M.; Gauthron, K.; Symonds, C.; Bloch, J.; Voisin, P.; Bellessa, J.; Lemaître, A.; Senellart, P. Evidence for confined tamm plasmon modes under metallic microdisks and application to the control of spontaneous optical emission. *Phys. Rev. Lett.* **2011**, *107*, 247402.
(18) Gazzano, O.; Michaelis de Vasconcellos, S.; Gauthron, K.; Symonds, C.; Voisin, P.; Bellessa, J.; Lemaître, A.; Senellart, P. Single photon source using confined tamm plasmon modes. *Appl. Phys. Lett.* **2012**, *100*, 232111.
(19) Parker, M.; Harbord, E.; Chen, L.; Clarke, E.; Kennedy, K.; Rarity, J.; Oulton, R. Telecommunication wavelength confined tamm plasmon structures containing InAs/GaAs quantum dot emitters at room temperature. *Phys. Rev. B: Condens. Matter Mater. Phys.* **2019**, *100*, 165306.
(20) Adams, M.; Cemlyn, B.; Henning, I.; Parker, M.; Harbord, E.; Oulton, R. A model for confined tamm plasmon devices. *J. Opt. Soc. Am. B* **2019**, *36*, 125.
(21) Leisher, P. O.; Raftery, J. J.; Kasten, A. M.; Choquette, K. D. Etch damage and deposition repair of vertical-cavity surface-emitting lasers. *J. Vac. Sci. Technol. B Microelectron. Nanometer Struct. Process. Meas. Phenom.* **2006**, *24*, 104−107.
(22) Ding, K.; Ning, C. Z. Fabrication challenges of electrical injection metallic cavity semiconductor nanolasers. *Semicond. Sci. Technol.* **2013**, *28*, 124002.
(23) Brückner, R.; Zakhidov, A. A.; Scholz, R.; Sudzius, M.; Hintschich, S. I.; Fröb, H.; Lyssenko, V. G.; Leo, K. Phase-locked coherent modes in a patterned metal−organic microcavity. *Nat. Photonics* **2012**, *6*, 322−326.
(24) Gessler, J.; Baumann, V.; Emmerling, M.; Amthor, M.; Winkler, K.; Höfling, S.; Schneider, C.; Kamp, M. Electro optical tuning of tamm-plasmon exciton-polaritons. *Appl. Phys. Lett.* **2014**, *105*, 181107.
(25) Liu, H.; Sun, X.; Yao, F.; Pei, Y.; Yuan, H.; Zhao, H. Controllable coupling of localized and propagating surface plasmons to tamm plasmons. *Plasmonics* **2012**, *7*, 749−754.
(26) Afinogenov, B. I.; Bessonov, V. O.; Nikulin, A. A.; Fedyanin, A. A. Observation of hybrid state of tamm and surface plasmon-polaritons in one-dimensional photonic crystals. *Appl. Phys. Lett.* **2013**, *103*, No. 061112.
(27) Lopez-Garcia, M.; Ho, Y.-L. D.; Taverne, M. P. C.; Chen, L.-F.; Murshidy, M. M.; Edwards, A. P.; Serry, M. Y.; Adawi, A. M.; Rarity, J. G.; Oulton, R. Efficient out-coupling and beaming of tamm optical states via surface plasmon polariton excitation. *Appl. Phys. Lett.* **2014**, *104*, 231116.
(28) Das, R.; Srivastava, T.; Jha, R. On the performance of tamm-plasmon and surface-plasmon hybrid-mode refractive-index sensor in metallo-dielectric heterostructure configuration. *Sens. Actuators, B* **2015**, *206*, 443−448.
(29) Azzini, S.; Lheureux, G.; Symonds, C.; Benoit, J.-M.; Senellart, P.; Lemaitre, A.; Greffet, J.-J.; Blanchard, C.; Sauvan, C.; Bellessa, J. Generation and spatial control of hybrid tamm plasmon/surface plasmon modes. *ACS Photonics* **2016**, *3*, 1776.
(30) Chestnov, I. Yu.; Sedov, E. S.; Kutrovskaya, S. V.; Kucherik, A. O.; Arakelian, S. M.; Kavokin, A. V. One-dimensional tamm plasmons: spatial confinement, propagation, and polarization properties. *Phys. Rev. B: Condens. Matter Mater. Phys.* **2017**, *96*, 245309.
(31) Ferrier, L.; Nguyen, H. S.; Jamois, C.; Berguiga, L.; Symonds, C.; Bellessa, J.; Benyattou, T. Tamm plasmon photonic crystals: from bandgap engineering to defect cavity. *APL Photonics* **2019**, *4*, 106101.

(32) Afinogenov, B.; Bessonov, V.; Fedyanin, A. Second-harmonic generation enhancement in the presence of tamm plasmon-polaritons. *Opt. Lett.* **2014**, *39*, 6895.
(33) Afinogenov, B.; Popkova, A.; Bessonov, V.; Lukyanchuk, B.; Fedyanin, A. Phase matching with tamm plasmons for enhanced second- and third-harmonic generation. *Phys. Rev. B: Condens. Matter Mater. Phys.* **2018**, *97*, na.
(34) Afinogenov, B. I.; Popkova, A. A.; Bessonov, V. O.; Fedyanin, A. A. Measurements of the femtosecond relaxation dynamics of tamm plasmon-polaritons. *Appl. Phys. Lett.* **2016**, *109*, 171107.
(35) Afinogenov, B. I.; Bessonov, V. O.; Soboleva, I. V.; Fedyanin, A. A. Ultrafast All-optical light control with tamm plasmons in photonic nanostructures. *ACS Photonics* **2019**, *6*, 844−850.
(36) Zhang, X.-L.; Song, J.-F.; Li, X.-B.; Feng, J.; Sun, H.-B. Optical Tamm states enhanced broad-band absorption of organic solar cells. *Appl. Phys. Lett.* **2012**, *101*, 243901.
(37) Zhang, X.-L.; Feng, J.; Han, X.-C.; Liu, Y.-F.; Chen, Q.-D.; Song, J.-F.; Sun, H.-B. Hybrid Tamm plasmon-polariton/microcavity modes for white top-emitting organic light-emitting devices. *Optica, OPTICA* **2015**, *2*, 579−584.
(38) Yang, Z.-Y.; Ishii, S.; Yokoyama, T.; Dao, T. D.; Sun, M.-G.; Pankin, P. S.; Timofeev, I. V.; Nagao, T.; Chen, K.-P. Narrowband wavelength selective thermal emitters by confined Tamm plasmon polaritons. *ACS Photonics* **2017**, *4*, 2212−2219.
(39) Wang, Z.; Clark, J. K.; Ho, Y.-L.; Vilquin, B.; Daiguji, H.; Delaunay, J.-J. narrowband thermal emission realized through the coupling of cavity and Tamm plasmon resonances. *ACS Photonics* **2018**, *5*, 2446−2452.
(40) Symonds, C.; Lheureux, G.; Hugonin, J. P.; Greffet, J. J.; Laverdant, J.; Brucoli, G.; Lemaitre, A.; Senellart, P.; Bellessa, J. Confined Tamm plasmon lasers. *Nano Lett.* **2013**, *13*, 3179−3184.
(41) Lheureux, G.; Azzini, S.; Symonds, C.; Senellart, P.; Lemaître, A.; Sauvan, C.; Hugonin, J.-P.; Greffet, J.-J.; Bellessa, J. Polarization-controlled confined Tamm plasmon lasers. *ACS Photonics* **2015**, *2*, 842−848.
(42) Symonds, C.; Azzini, S.; Lheureux, G.; Piednoir, A.; Benoit, J. M.; Lemaitre, A.; Senellart, P.; Bellessa, J. High quality factor confined tamm modes. *Sci. Rep.* **2017**, *7*, 1−7.
(43) Dang, G. T.; Kanbe, H.; Taniwaki, M. Photoluminescence of an Al0.5Ga0.5As/GaAs multiple quantum well in the temperature range from 5 to 400 K. *J. Appl. Phys.* **2009**, *106*, No. 093523.
(44) Johnson, P. B.; Christy, R. W. Optical constants of the noble metals. *Phys. Rev. B* **1972**, *6*, 4370−4379.
(45) Gehrsitz, S.; Reinhart, F. K.; Gourgon, C.; Herres, N.; Vonlanthen, A.; Sigg, H. The refractive index of AlxGa1−xAs below the band gap: accurate determination and empirical modeling. *J. Appl. Phys.* **2000**, *87*, 7825−7837.

https://dx.doi.org/10.1021/acsphotonics.0c00781
ACS Photonics 2020, 7, 2952−2957